Aust. J. Phys., 1995, **48**, 439–52

Modeling and Measurement of Submicron Particles in RF Plasmas in Ar*

Y. Hosokawa,[A] *T. Kitajima and T. Makabe*

Department of Electrical Engineering, Faculty of Science and Technology,
Keio University, 3-14-1 Hiyoshi, Yokohama 223, Japan.
[A] Permanent address; Mechanical Engineering Research Laboratory,
Kobe Steel Ltd, 1-5-5 Takatukadai, Kobe, Japan.

Abstract

The work is focused on the growth and transport of submicron particles in nonreactive radiofrequency plasma in Ar at 13·56 MHz, studied by numerical modeling using the relaxation continuum model, and by experiment using spatiotemporally resolved optical emission spectroscopy with Mie scattering. The particle growth/decay under conditions of the initially injected $(CF_2)_n$, and the related spatiotemporal change of the rf plasma structure, are discussed in terms of their numerical and experimental results. The results give suggestions with respect to the influence of particles in a dusty rf plasma system, such as dry etching and sputtering.

1. Introduction

The appearance of submicron particles has been widely observed in plasma processing reactors for sputtering, deposition and etching during the past decade (Selwyn *et al.* 1990). The particle size and density in a growth process have been detected in a range greater than 10 nm by using Mie scattering of laser light (Watanabe *et al.* 1992). A correlation between particle growth and spatiotemporal plasma structure was roughly measured in a parallel plate radiofrequency (rf) reactor at 13·56 MHz (Kamata *et al.* 1994).

The particles in rf plasmas, maintained between parallel plates, are essentially subject to two well-known processes. They are *surface charging* and *spatial trapping*. The total surface charge on a particle is always negative, and the amount of negative charge on the particle in electropositive gases is higher than that in electronegative gases even for the same plasma density. After charging, the massive negative ion is confined within bulk plasma by the strong positive ion sheath field in front of both electrodes at a pressure of greater than half a Torr. Under these circumstances, the growing process of nanometre-particles may be substantial.

The present study is focused on the growth and transport of submicron particles, observable by the Mie scattering technique. The rf discharge involving a submicron particle growth is numerically modeled as well as observed optically and electrically. In doing so, the initial source of particles and composition of the rf discharge is carefully chosen. That is, $(-CF_2CF_2-)_n$ and its fragments are prepared with Ar rf sputtering from the teflon plate surrounding Al electrodes in advance of the measurement. The rf sputtering voltage is carefully controlled so

0004-9506/95/030439$05.00

that the Al electrode surface is not influenced by sputtering. After preparation of $(-CF_2CF_2-)_n$ and its fragments on the bottom of the reactor between both electrodes, the gas is replaced. When this preparation procedure is followed, the laser light scattering onset time and the succeeding temporal behaviour of the signal are reproducible within a scatter of 10% up to 600 s after the initiation of the discharge.

In order to theoretically investigate particle growth in the experimentally detectable range, i.e. submicron scale, we model the subsystem of heavy particles with initial mass M_0 and number density N_{p0} as homogeneously dispersed into the periodic steady state rf glow discharge. The system, initially consisting both of the subsystem with electrons and positive ions and that with heavy particles, is numerically simulated by using the *extended relaxation continuum* (RCT) *model* (Makabe *et al.* 1992; Nakano *et al.* 1994). It is assumed that for the low density of the initial particles N_{p0}, collisions between heavy particles are negligible compared with the heavy particle–atmospheric light atom interaction. Then, the collision between a particle and an atom is considered by the Maxwell model, that is, through dipole interaction occuring only at impact. The swarm parameters of the massive particles with negative charge are assumed to be given by the Wannier (1953) expression as a function of the reduced field temporally averaged over one cycle. Even for this simple model, it seems that no numerical results exist dealing with the spatiotemporal change of rf plasma structure involving the growth of dust particles.

As mentioned above, a heavy particle in the plasma has the property of being negatively charged. In this sense, the present rf discharge system simultaneously realises two kinds of interesting transport of negative charges, that of electrons and of negatively charged massive ions from the viewpoint of the mass ratio between charged particle and neutral molecule, m/M. One is the Lorentz limit for electrons ($m/M \ll 1$), and the other the Rayleigh limit for the massive ions ($m/M \gg 1$).

In this paper, we investigate an rf plasma structure including a particle growth/decay process both by numerical modeling using the extended RCT model and by space- and time-resolved optical emission spectroscopy (STR OES) (Tochikubo and Makabe 1991). The experimental apparatus and the system are similar to those described in a previous paper (Kamata *et al.* 1994).

2. Modeling of Dusty Plasmas

The rf plasma system including particle growth, decay and charging is modeled with the following approximations:

(1) No thermal gradient exists in the discharge including electrode (Jellum *et al.* 1991).
(2) Electron transport is not affected by the presence of particles, except through the modified electric field.
(3) Particle transport is considered by the induced-dipole interaction with the neutral molecule, i.e. through the application of Wannier's (1953) theory under the temporally averaged field, although the interaction between particles themselves is ignored.
(4) Monodisperse characteristics in particle diameter are considered (Boufendi *et al.* 1992).

(5) One-dimensional spatially resolved rf structure with temporal modulation is modeled similar to our previous measurement (Kamata *et al.* 1994).
(6) Momentum transfer of positive ions to the particle is negligible at pressures higher than half a Torr (Barnes *et al.* 1992).

We develop our relaxation continuum model (Makabe *et al.* 1992) to the system with positive ions, electrons, and negatively charged massive particles under these simplifications. Then, we have to consider the momentum balance of positive ions as well as electrons, since part of the current is carried by massive ions in electronegative rf plasmas (Nakano *et al.* 1994).

(2a) Governing Equations for the Transport of Charged Particles

Charged particle continuity:

$$\frac{\partial}{\partial t}n_e(z,t) = k_i N n_e - \frac{\partial}{\partial z}\left(n_e v_{de} - D_{Le}\frac{\partial n_e}{\partial z}\right), \tag{1}$$

$$\frac{\partial}{\partial t}n_p(z,t) = k_i N n_e - \frac{\partial}{\partial z}\left(n_p v_{dp} - D_{Lp}\frac{\partial n_p}{\partial z}\right), \tag{2}$$

$$\frac{\partial}{\partial t}n_d(z,t) = -\frac{\partial}{\partial z}\left(n_d v_{dd} - D_{Ld}\frac{\partial n_d}{\partial z}\right). \tag{3}$$

Charged particle momentum relaxation:

$$\frac{\partial}{\partial t}(m_e v_{de}) = eE - k_{me} N m_e v_{de} - m_e v_{de}\frac{\partial v_{de}}{\partial z}, \tag{4}$$

$$\frac{\partial}{\partial t}(m_p v_{dp}) = eE - k_{mp} N m_p v_{dp} - m_p v_{dp}\frac{\partial v_{dp}}{\partial z}. \tag{5}$$

Energy relaxation of electrons with $\epsilon \geq \epsilon_i$:

$$\frac{\partial}{\partial t}(n_e E_{eff}^2) = -\frac{E_{eff}^2 - E^2}{\tau_{\epsilon i}}n_e - \frac{\partial}{\partial z}\left(n_e v_{de} E_{eff}^2 - D_{Le}\frac{\partial (n_e E_{eff}^2)}{\partial z}\right). \tag{6}$$

Poisson's equation:

$$\frac{\partial E(z,t)}{\partial z} = \frac{e}{\epsilon_0}(n_p - n_e - q_e n_d), \tag{7}$$

where, n_e, n_p, n_d and N are the number density of the electrons, positive ions Ar^+, negatively charged particles, and neutral Ar, respectively. The mass and charge of the electron and Ar^+ are, respectively, given by m_e, m_p and e. Surface charge of the particle is denoted by q_e, k_i is the ionisation rate coefficient, and v_{de}, v_{dp} and v_{dd} are the drift velocities of electrons, Ar^+ and negatively charged

particles. Also, D_{Le}, D_{Lp} and D_{Ld} are the longitudinal diffusion coefficients of electrons, Ar^+ and particles respectively (Makabe *et al.* 1992), k_{me} and k_{mp} are the momentum transfer rate coefficients of electrons and Ar^+, $E(z,t)$ is the instantaneous local electric field, and $E_{eff}(z,t)$ is the effective field for ionisation with time constant $\tau_{\epsilon i}$.

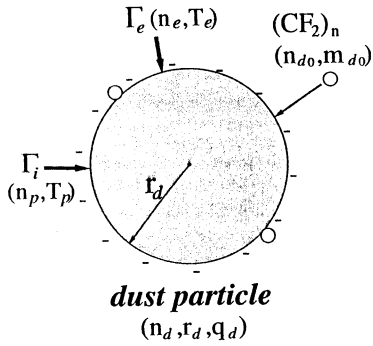

Fig. 1. Fluxes incident on the surface of a dust particle from the plasma.

(2b) Governing Equation on the Particle Surface

A dielectric particle in a plasma will be influenced by various kinds of fluxes on the surface. Here, it will be sufficient to consider three kinds of particle flux, i.e. electron, positive ion and $(CF_2)_n$ under the present simplifications (see Fig. 1). The total amount of surface charge q_d is determined from (Nowlin and Carlile 1991):

$$\frac{\partial}{\partial t} q_d(t) = 4\pi r_d^2 e\{\Gamma_e - \Gamma_p\}\,, \tag{8}$$

where

$$\Gamma_e = \frac{n_e}{4}\sqrt{\frac{8kT_e}{\pi m_e}}\exp\left(\frac{q_d e}{4\pi\epsilon_0 r_d k T_e}\right), \tag{9}$$

$$\Gamma_p = \frac{n_e}{4}\sqrt{\frac{8kT_p}{\pi m_p}}\left(1 - \frac{q_d e}{4\pi\epsilon_0 r_d k T_p}\right), \tag{10}$$

k_B is Boltzmann constant, and T_e and T_p are the temperatures of electrons and Ar^+ respectively. The particle radius is denoted by r_d. Fluxes of electrons and positive ions will be balanced on the surface with time constant τ_c. Then both fluxes satisfy the relation

$$\Gamma_e - \Gamma_p = 0\,. \tag{11}$$

It is demonstrated from previous experimental work that the monodisperse particle growth is realised with a rate coefficient independent of time in the present system (Kamata *et al.* 1994). This implies a growth mechanism where small $(CF_2)_n$ accumulates on the surface of a big particle. Under the circumstances,

the growth equation of the particle is related to the thermal velocity v_{d0}, mass m_{d0}, and number density n_{d0} of $(CF_2)_n$, and the particle radius is written as a function of time as

$$\frac{d}{dt}r_d(t) = \frac{1}{4\rho_d} k n_{d0} v_{d0} m_{d0}\,, \tag{12}$$

where ρ_d is the density of the particle. The right-hand side of equation (12) is estimated at $2{\cdot}33\ \mathrm{nm\,s^{-1}}$ from the previous measurement (Kamata *et al.* 1994).

(2c) Governing Equation in Particle Decay Process

For the decay of particles, we only consider the exponential decay process with single time constant, observed in the previous measurement, that is,

$$n_d(z,t) = n_{d0} \exp(-t/43{\cdot}4)\,. \tag{13}$$

This is rather artificial in this modeling, since the experimental parallel plate plasma reactor is set horizontally, and then the massive particle disappears from the centre part of the discharge axis where the measurement is focused.

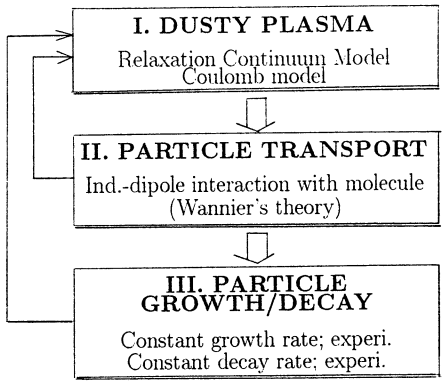

Fig. 2. Time-chart in the simulation of an rf plasma structure including particle growth/decay processes.

When an rf discharge driven by 13·56 MHz waves involves growth of particles and decay processes, we have to consider the great difference in time constants between the transport of electrons, ions and particles, charging, and particle growth and their density decay. It will be reasonable to divide the time development of the rf dusty plasma into three stages. These are:

(i) Redistribution of the rf plasma structure due to charging on stationary particles. Periodic steady state plasma structure (short time behaviour) will appear after establishment of charging.
(ii) Particle transport under the time averaged spatial field.
(iii) Long-time growth/decay of particles in rf plasma.

These stages are shown in the time-chart in Fig. 2. In stage I, equations (1) (2), (4)–(7) are numerically solved with $\Delta t_1 = 9{\cdot}2{\times}10^{-11}$ s and $\Delta z = 0{\cdot}4$ mm. The particle transport equation (3) in stage II is computed with a large time step $\Delta t_2 = 10^{-6}$ s and $\Delta z = 0{\cdot}4$ mm. Long-time development of particles in stage III is solved from (12) and (13) with time step $\Delta t_3 = 10$ s and $\Delta z = 0{\cdot}4$ mm.

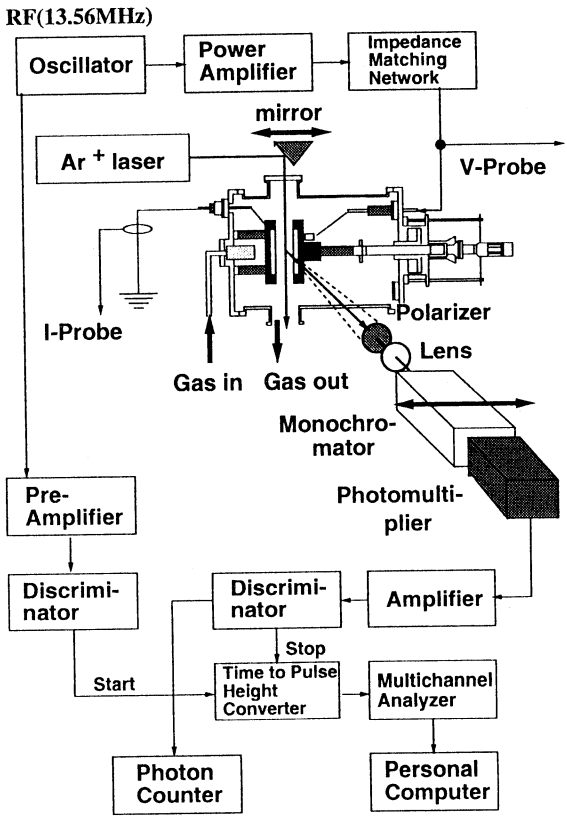

Fig. 3. Schematic illustration of the experimental apparatus and the detector system.

3. Experimental Procedure

The experimental apparatus, measurement system and procedure were described in a previous paper (Kamata *et al.* 1994). Here we only summarise. Parallel plate aluminum electrodes of 8 cm diameter are positioned with 2 cm spacing in the centre of the stainless steel chamber 20 cm in diameter (see Fig. 3). The time and axial space resolutions are, respectively, 0·2 ns and 1 mm. Emitted photons within 2 cm of the central axis of the discharge are detected by using the photon counting technique. That is, the emission intensity $\Phi_{jk}(z,t)$ ($\mathrm{cm}^{-3}\,\mathrm{s}^{-1}$) from state j to k is expressed under the condition that the radiative lifetime τ_{rad} is much shorter than the time constant of diffusion, τ_D, as

$$\Phi_{jk}(z,t) = k_0 \int_{-\infty}^{t} \frac{\Lambda_j(z,t')}{\tau_{rad}} \exp\left(-\frac{t-t'}{\tau_{eff}}\right) \mathrm{d}t' , \tag{14}$$

where $\Lambda_j(z,t)$ ($\mathrm{cm}^{-3}\,\mathrm{s}^{-1}$) is the net excitation rate to state j, and τ_{eff} the effective lifetime considering the self-quenching. Further k_0 is a constant showing the instrumental function. We can estimate τ_{eff} under the condition that the overall profile of the net excitation rate has a non-negative value—τ_{eff} of excited

$Ar(3p_5)$ is estimated at 50 ns. The absolute net excitation rate by electron impact is obtained by a deconvolution procedure in (14) from STR OES in the calibrated detection system. At the same time, the actual power dissipated in the rf discharge is observed from the current and sustaining voltage wave forms, which are sampled from the current and high-voltage probes. The current was monitored between the grounded electrode and the ground.

An unpolarised Ar^+ ion laser ($\lambda = 488$ nm) with beam diameter of 0·62 mm is used as a coherent light source and directed to the mirror mounted on the movable stage controlled by computer, which allows us to execute spatially resolved scattering measurements. The laser light enters the discharge parallel to the electrodes from the top window. The measurement by the photon counting technique is employed for the detection of the laser beam scattered by 90° as well as the emission of excited species in the discharge. The scattered laser intensities parallel and perpendicular to the scattered plane, $I_\perp$ and $I_{||}$, can be observed individually by inserting a polariser between the scattered beam and the lens system in front of the monochromator shown in Fig. 3.

Thus, we employ a technique based on Mie scattering theory by unpolarised laser in order to measure particles in situ (Bohren and Huffman 1983). It is assumed that the particle is made from $(-CF_2CF_2-)_n$ with monodispersion in size and refractive index of 1·35. The experimental scattering intensities $I_{\perp,||}$ are influenced by both the instrumental function of the detector system and the scattering angular distribution. The calibration of $I_{\perp,||}$ is also performed beforehand in the manner similar to Tochikubo and Makabe (1991).

The particle size with monodispersion is estimated from the ratio of $I_\perp$ to $I_{||}$ by using Mie scattering theory (Bohren and Huffman 1983; Watanabe *et al.* 1993). In particular, the particle radius r_p larger than 250 nm is estimated by comparing the theoretical $I_{\perp,||} - r_p$ characteristics with the experimental $I_{\perp,||}$ peaks against the time from the onset of the discharge. Then, the particle number density is given from the absolute scattering intensity using the particle radius mentioned above.

4. Results and Discussion

The numerical simulation of the rf plasma involving a particle growth/decay process has been performed by using the RCT model under the conditions, $V_0 = 60$ V, $f = 13{\cdot}56$ MHz and $p = 1$ Torr in Ar. The external discharge parameters coincide with those in our experimental with gas flow rate of 10 sccm. In particular, the initial particles with a radius r_d of 100 nm and number density 10^7 cm^{-3} are uniformly distributed between both electrodes, except for a 2 mm region from the plates under the circumstances of an infinite number of $(CF_2)_n$. That is, in this work we simulate the particle growth/decay and the change of the spatiotemporal rf plasma structure after the injection of the particle. The initial scale and the density are identified by the present experimental work.

We first investigate the short-time development, that is, the change of spatiotemporal distributions of electrons, Ar^+ and particles, just after the injection of dielectric particles into the Ar rf plasma. The transient phenomena are only influenced by the lack of electrons in the discharge due to charging on the dielectric particle surface. Fig. 4 shows a chain of dependence between the charging and the spatiotemporal profiles at $\omega t = 3\pi/2$ ($t = 0$ means the steady

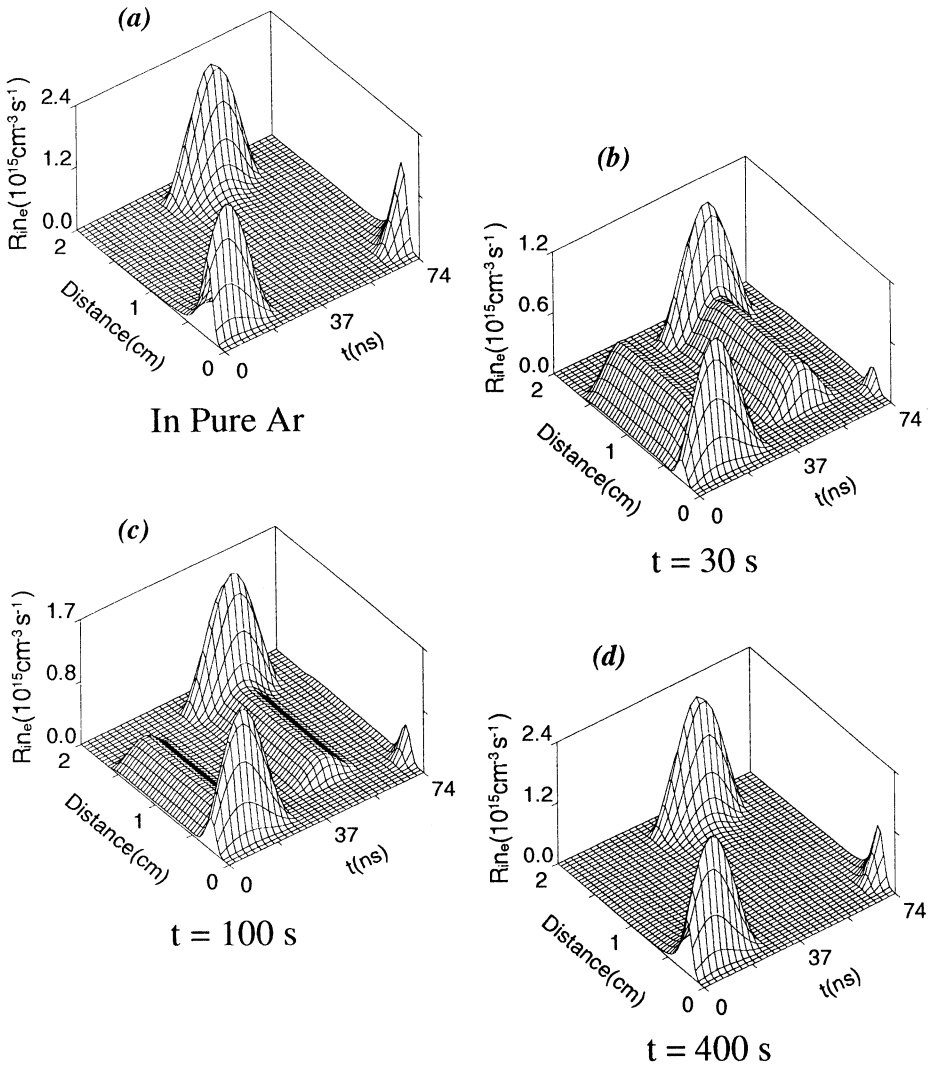

Fig. 6. Spatiotemporal net ionisation rate during one cycle in Ar including the dust particle growth/decay processes. The external conditions are the same as in Fig. 4: (*a*) in pure Ar (initial steady state condition), (*b*) at the most affected phase in the external electrical characteristics (30 s after the injection), (*c*) at 100 s after particle injection and (*d*) when almost recovered (400 s after the injection).

state profile of the rf discharge in pure Ar under the above external condition. A sudden decrease of the electron density during the first one hundred cycles is followed by a gradual increase of the electron density, while the positive ion density monotonically increases in time (see Figs 4*b* and 4*c*). These characteristics result from the difference between the gain/loss processes between electrons and positive ions due to the collisional ionisation and outflow loss. As a result, it is found that the time constant for charging on the particle surface, injected neutrally into the discharge, is approximately 0·1 ms (see Fig. 4*a*). Then, the relation (11) is satisfied in a time-averaged fashion.

The long-time development in the preset dusty rf plasma system is demonstrated at $\omega t = 3\pi/2$ in Fig. 5 in terms of the electron, Ar^+ and particle charge densities. With the disappearance of the large particle from the discharge volume, the electron density increases slowly and recovers the original spatial profile in pure Ar. On the other hand, the positive ion density has almost the superimposed profile of the particle charge density over the original distribution in pure Ar. This discrepancy between the electron and positive ion temporal profile comes from the great difference in the mobility in the presence of the rf field at 13·56 MHz. The positive ion sheath results from the relation between electrons and positive ions in front of the electrodes, although the two kinds of negative species, i.e. electrons and particles, are distributed over space in a different way. The overall time constant for recovery is estimated to be 400 s.

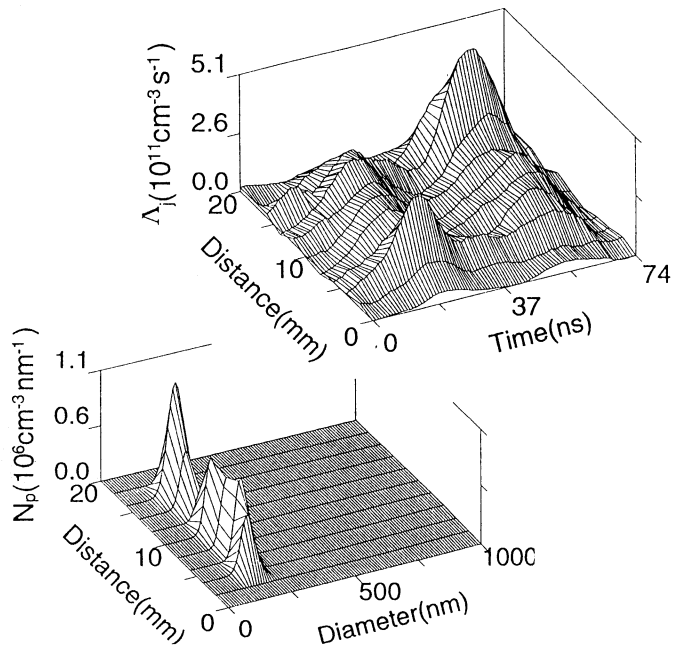

Fig. 7. Experimental net excitation rate of Ar ($3p_5$; $\epsilon = 14{\cdot}6$ eV) and particle diameter–density distribution 100 s after particle injection. External discharge conditions are the same as in Fig. 4 except for the gas flow rate of 10 sccm (standard cm^3 per min).

The negatively charged particles are confined in the bulk plasma between both positive ion sheaths in front of the electrodes, and strongly change the spatiotemporal distributions both of the electrons and of the electric field. Therefore, it is very important to investigate the influence of the particle growth on the net production rate of active species in material processing in a parallel plate reactor. Fig. 6 exhibits the change of the net rate in the ionisation during one cycle. Fig. 7 shows the experimental net excitation rate of $Ar(3p_5)$ with threshold energy of 14·6 eV and the particle density distribution at 100 s, after the particle grows up to 100 nm in pure Ar for $V_0 = 60$ V, $f = 13{\cdot}56$ MHz,

$p = 1$ Torr and $S = 10$ sccm. The experimental net rate is in qualitatively good agreement with the numerical value in Fig. 6*c*, although the observed profile is broader in time and space. The particle distribution exhibits the monodisperse size characteristics, and it is almost uniform spatially. The detailed experimental results will be discussed elsewhere (Kitajima and Makabe 1994).

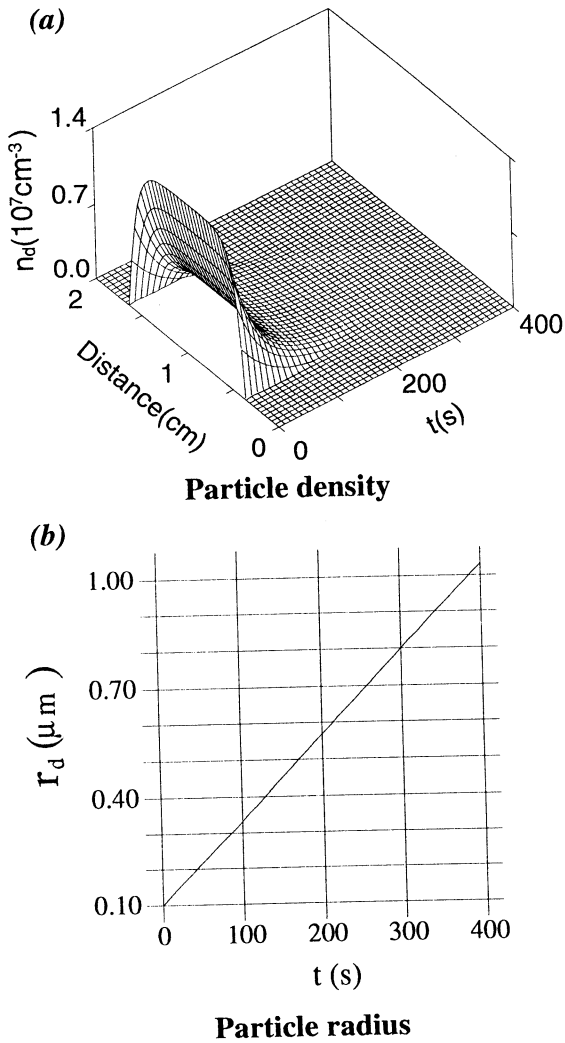

Fig. 8. Space- and time-dependence of (*a*) the particle density and (*b*) the particle radius.

The net ionisation rate under the presence of particles shows the intermediate characteristics between that of electropositive gases and of electronegative gases. That is, the maximum of the net rate arises from the reflected electrons in front of the electrode at cathodic phase, as is shown in electropositive gases (Tochikubo *et al.* 1990). Also the existence of the ionisation in the bulk plasma is similar to that in electronegative gases (Makabe *et al.* 1990; Petrovic *et al.*

1993). The net rate just in front of the instantaneous anode due to double layer formation is not found in the numerical Figs 6*b* and 6*c* or in the experimental Fig. 7*a*. This results from the fact that a double layer is not formed, since the negatively charged particle is confined in a relatively low field region far from the electrodes, compared with the spatial distribution of negative ions in electronegative rf plasmas (Petrovic *et al.* 1993; Nakano *et al.* 1994). The time and position of the peak in Figs 6*b* and 6*c* is little affected by the presence of particles as compared with that in Fig. 6*a* in pure Ar. These are the result of the weak electronegativity arising from the negatively charged massive particles.

Finally, as for the dust particle in Ar rf discharge, we show the space- and time-dependence of the density and the radius of particles. The monodisperse linear growth of the particles in Fig. 8*b* is assumed beforehand and it is supported by our experimental results in Fig. 7*b*. The particle, injected uniformly between $z = 2$ and 18 mm, continues to change the spatial profile with a very long time constant under the influence of first charging and successive trapping within the bulk plasma by the positive ion sheath in front of both electrodes. At the same time, under these circumstances, the particle volume growth and the density decay arise in chemically nonreactive Ar rf plasma. The atomic composition of the particle is analysed after the discharge by an Electron Probe Micro Analyser (EPMA), and C and F atoms are detected. Also the CF bond is detected by FT-IR analysis.

The present results give some suggestions with respect to the influence of particles in a dusty plasma system, such as plasma processing. It is emphasised through the present study that a systematic investigation of ion transport in an rf field is greatly needed.

Acknowledgments

This work was supported in part by a Grant-in-Aid for Scientific Research No. B05452106 from the Ministry of Education, Science and Culture in Japan.

References

Barnes, M. S., Keller, J. H., Forster, J. C., O'Neil, J. A., and Coultas, D. K. (1992). *Phys. Rev. Lett.* **68**, 313.

Bohren, C. F., and Huffman, D. R. (1983). 'Absorption and Scattering of Light by Small Particles' (Wiley: New York).

Boufendi, L., Plain, A., Blondeau, J. Ph., Bouchoule, A., Laure, C., and Toogood, M. (1992). *Appl. Phys. Lett.* **60**, 169.

Jellum, G. M, Daugherty, G. E., and Graves, D. B. (1991). *J. App. Phys.* **69**, 6923.

Kamata, T., Kakuta, S., Yamaguchi, Y., and Makabe, T. (1994). *Plasma Source Sci. Technol.* **3**, 310.

Kitajima, T., and Makabe, T. (1994). *Bull. Am. Phys. Soc.* **39**, 1492.

Makabe, T., Nakano, N., and Yamaguchi, Y. (1992). *Phys. Rev.* A **45**, 2520.

Makabe, T., Tochikubo, F., and Nishimura, M. (1990). *Phys. Rev.* A **42**, 3674.

Nakano, N., Shimura, N., and Petrovic, Z. Lj. (1994). *Phys. Rev.* E **49**, 4455.

Nowlin, R. N., and Carlile, R. N. (1991). *J. Vac. Sci. Technol.* A **9**, 2825.

Petrovic, Z. Lj., Tochikubo, F., Kakuta, S., and Makabe, T. (1993). *J. Appl. Phys.* **73**, 2163.

Selwyn, G. S., Heidenreich, J., and Haller, K. L. (1990). *Appl. Phys. Lett.* **57**, 1876.

Tochikubo, F., and Makabe, T. (1991). *Meas. Sci. Technol.* **2**, 1133.

Tochikubo, F., Kokubo, T., Kakuta, S., Suzuki, A., and Makabe, T. (1990). *J. Phys.* D **23**, 1184.

Wannier, G. H. (1953). *Bell Syst. Tech. J.* **32**, 170.

Watanabe, Y., Shiratani, M., and Yamashita, M. (1992). *Appl. Phys. Lett.* **61**, 1510.
Watanabe, Y., Shiratani, M., and Yamashita, M. (1993). *Plasma Sources Sci. Technol.* **2**, 35.

Manuscript received 28 October 1994, accepted 26 April 1995